

Defect-Dipole Formation in Copper-Doped PbTiO₃ Ferroelectrics

Rüdiger-A. Eichel,^{1,*} Paul Erhart,^{2,3} Petra Träskelin,⁴ Karsten Albe,³ Hans Kungl,⁵ and Michael J. Hoffmann⁵

¹*Eduard-Zintl-Institut, Technische Universität Darmstadt, D-64287 Darmstadt, Germany*

²*Lawrence Livermore National Laboratory, Livermore, California 94550, USA*

³*Institut für Materialwissenschaft, Technische Universität Darmstadt, D-64287 Darmstadt, Germany*

⁴*University of California, Davis, California 95616, USA*

⁵*Institute of Ceramics in Mechanical Engineering, University of Karlsruhe, D-76131 Karlsruhe, Germany*

(Received 15 August 2007; published 6 March 2008)

The defect structure of hard copper-modified polycrystalline PbTiO₃ ferroelectrics is investigated by means of electron paramagnetic resonance and hyperfine sublevel correlation spectroscopy, as well as density functional theory calculations. Special emphasis is put on the ²⁰⁷Pb-hyperfine couplings, which are resolved up to the third coordination sphere. The results prove that copper is incorporated at the octahedrally coordinated Ti site, acting as an acceptor. Because of charge compensation the formation of Cu impurity–oxygen vacancy pairs is energetically very favorable. The corresponding (Cu_{Ti}^{II}-V_O^{••})[×] defect dipole is found to be orientated along the [001] axis.

DOI: 10.1103/PhysRevLett.100.095504

PACS numbers: 61.72.J-, 61.72.Bb, 85.50.-n

Piezoelectric lead zirconate titanate Pb[Zr_xTi_{1-x}]O₃, (PZT $x/1-x$) ceramics are the materials of choice for various applications, ranging from sensors and actuators with superior electromechanical properties [1] to non-volatile memory devices [2]. The piezoelectric properties are typically tailored by means of doping with aliovalent transition metal or rare-earth ions. In the case of acceptor doping this usually implies an increasing concentration of oxygen vacancies for charge compensation, which in turn may form defect associates with the dopants. More specifically, such defect dipoles act as centers of anisotropy, which affect the polarization of the surrounding unit cells and potentially impede polarization reversal [3]. It has been proposed that these dipoles can cooperatively align along a certain crystallographic direction, giving rise to a macroscopically detectable *internal bias field* [4,5]. In fact, experiments have been reported that indicate a gradual alignment of (Fe_{Ti}^I-V_O^{••})[•] defect dipoles in BaTiO₃ and PZT [6,7]. A basic mechanism based on the realignment of these defect dipoles has been proposed to describe the ferroelectric aging phenomenon [8]. This model relates the nonreversible domain switching in ferroelectrically aged ceramics to the transformation of dipolar defects, in which the defect symmetry follows the crystal symmetry. It is widely accepted that oxygen vacancies and their associates with impurities and/or dopants have an important impact on the macroscopic ferroelectric response of a material. Our understanding of the effect of dopants on the microscopic structure as well as the connection to macroscopic properties is, however, still very incomplete.

Iron-doped compounds have received particular attention because in the case of the high-spin ($S = \frac{5}{2}$) Fe³⁺ functional center, the inherent fine-structure interaction can be exploited to probe the local crystal field. They have been shown to form (Fe_{Zr,Ti}^I-V_O^{••})[•] defect dipoles [6,7,9–13]. In the case of the ($S = \frac{1}{2}$) Cu²⁺ center such an analysis is hampered due to the absence of a fine-

structure interaction. Therefore, in studies on Cu-modified material a more indirect argumentation has been pursued [14,15], and the observation of an isotropically distributed electron spin density lead to the suggestion that nonassociated Cu_{Zr,Ti}^{II} ions prevail.

The goal of this Letter is to develop a consistent picture of acceptor doping in piezoelectrics, by a combination of experimental and theoretical methods. To this end, we employ hyperfine sublevel correlation (HYSCORE) spectroscopy [16] for probing weak ²⁰⁷Pb hyperfine couplings to the Cu²⁺ center in conjunction with density functional theory (DFT) calculations to analyze the spin-density patterns of various conceivable defect configurations.

Experimental.—Details of the sample preparation by a standard mixed-oxide route are given elsewhere [14]. The X-band pulse electron paramagnetic resonance (EPR) measurements were performed at 9.7 GHz on a Bruker ElexSys 680 spectrometer at a temperature of 10 K. The field-swept free induction decay (FID) detected EPR spectrum was obtained as a function of a highly selective microwave pulse of 500 ns duration. HYSCORE spectra were recorded using a standard four-pulse sequence ($\frac{\pi}{2} - \tau - \frac{\pi}{2} - t_1 - \pi - t_2 - \frac{\pi}{2} - \tau$ -echo) and an eight-step phase cycle [17]. Pulse lengths of $t_{\pi/2} = t_{\pi} = 16$ ns and a delay time of $\tau = 400$ ns were employed. A more detailed description of the experimental setup and the applied microwave pulse sequences can be found in [14].

Theory.—An appropriate theoretical description of the EPR and HYSCORE spectra for an unpaired $3d^9$ electronic configuration with spin $S = \frac{1}{2}$ interacting with N nuclei of arbitrary spin I is based on the following spin Hamiltonian

$$\mathcal{H} = \beta_e \mathbf{B}_0 \cdot \mathbf{g} \cdot \mathbf{S} - \beta_n \sum_{i=1}^N g_{n,i} \mathbf{B}_0 \cdot \mathbf{I}_i + \sum_{i=1}^N \mathbf{S} \cdot \mathbf{A}_i \cdot \mathbf{I}_i \quad (1)$$

The $g_{n,i}$ are the corresponding nuclear g factors, while β_e

and β_n are the Bohr and nuclear magnetons, respectively. The first and second term are the electronic and nuclear Zeeman interaction, respectively, where \mathbf{B}_0 denotes the external field. The last term corresponds to the hyperfine interactions due to nearby magnetic nuclei. The hyperfine tensors \mathbf{A}_i as well as the external field \mathbf{B}_0 are given in the principal axes system of the \mathbf{g} matrix, and the index i refers to a particular nucleus. The copper nuclear quadrupole interaction was not resolved in the spectra and thus has been neglected.

In general, the hyperfine interactions \mathbf{A}_i may be expressed as $\mathbf{A}_i = a_{\text{iso},i} \mathbf{1} + \mathbf{A}'_i$, where $a_{\text{iso},i}$ is the isotropic hyperfine coupling constant and the traceless and symmetric tensor \mathbf{A}'_i describes the anisotropic dipole-dipole interaction between the electron spin \mathbf{S} and the nuclear spin \mathbf{I}_i . Since the second-rank tensors \mathbf{A}'_i are traceless and symmetric, there is always a coordinate system in which the tensor is diagonal with the elements A'_{\perp} and $A'_{\parallel} = -2A'_{\perp}$. By convention, A'_{\parallel} is taken to be the principal value with the largest absolute magnitude. Therefore, the dipolar hyperfine interaction can be described in terms of the single parameter A'_{\parallel} , which represents the dipolar hyperfine coupling constant.

In order to transform the spin-Hamiltonian parameters into structural information, a point-dipole approximation can be assumed, where the dipolar hyperfine parameter A'_{\parallel} scales with r^{-3} ,

$$A'_{\parallel} = \frac{\mu_0}{4\pi} \frac{g g_n \beta_e \beta_n}{r^3 h}. \quad (2)$$

This equation provides an estimate for the distance r between the paramagnetic center and the corresponding magnetic nucleus.

Computational details.—DFT calculations within the local spin-density approximation were carried out using the projector-augmented wave method as implemented in the Vienna *ab initio* simulation package (VASP) [18,19]. The $5d$ electrons of Pb, the $3s$ and $3p$ electrons of Ti, and the $4d$, $3d$, and $3p$ of Cu were included as semicore states. All calculations were carried out using Gaussian smearing with a width of 0.2 eV and a $4 \times 4 \times 4$ Monkhorst-Pack mesh for Brillouin zone sampling [20]. In order to model the defect configurations, supercells containing $2 \times 2 \times 2$ to $2 \times 2 \times 4$ unit cells equivalent to 40 to 80 atoms were employed, and a variety of different defect configurations and charge states was explored. Further details can be found in [21].

Results and discussion.—The FID-detected EPR spectrum of Cu^{2+} -doped PbTiO_3 at 10 K is shown in Fig. 1(a) and can be described by an axially symmetric g matrix with diagonal elements $g_{\parallel} = 2.332 > g_{\perp} = 2.049 > g_e = 2.0023$ and $A^{63\text{Cu}}$ -hyperfine tensor with diagonal elements $A'_{\parallel} = 395$ MHz, $A'_{\perp} = 20$ MHz [22]. This situation is characteristic for Cu^{2+} centers in octahedral coordination

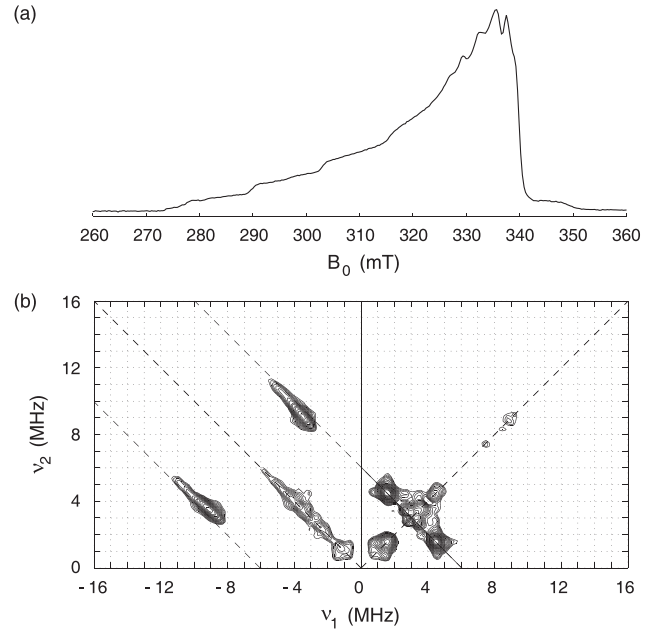


FIG. 1. (a) FID-detected X-band EPR spectrum of 0.25 mol % doped $\text{Cu}^{2+}:\text{PbTiO}_3$ recorded at 10 K. (b) X-band ^{207}Pb -HYSCORE spectrum recorded at 10 K and observer position of 337.7 mT.

distorted along one of the pseudocubic axes [23–27]. Adopting a fully ionic picture, this implies that copper dopants act as acceptor-type centers and create holes in the valence band. Our DFT calculations of isolated Cu centers are in full agreement with this experimental observation, showing that in acceptor-doped compounds the most stable charge state leads to two holes in the valence band equivalent to a $\text{Cu}_{\text{Ti}}^{\prime\prime}$ state [21].

Moreover, the DFT calculations give evidence for a reduction of the distance along [001] between the Cu^{2+} ion and the nearest oxygen plane to 0.20 Å compared to 0.26 Å (Ti-O) in the ideal structure. Figure 2(c) shows that the spin density for this configuration is mostly localized at the Cu^{2+} ion, which correlates with an asymmetry in the density of states of the Cu- $3d$ electrons [21]. It is, furthermore, apparent that the spin-density distribution at the copper site possesses tetragonal symmetry, in agreement with the observed axially of the Cu^{2+} g matrix and the $A^{63\text{Cu}}$ -hyperfine tensor.

The displacement of the Cu^{2+} -functional center in the unit cell can be estimated from the HYSCORE results. This is achieved by assuming a point-dipole approximation to analyze the dipolar ^{207}Pb -hyperfine interactions of the copper functional center with the surrounding lead nuclei. A representative spectrum along the g_{\perp} orientation is illustrated in Fig. 1(b). The correlations in the spectrum appear as off-diagonal cross peaks, providing the identity of the nucleus through the nuclear Larmor frequency ν_1 as well as its hyperfine coupling [14]. The observed spectrum exclusively consists of signals from the ^{207}Pb isotope of

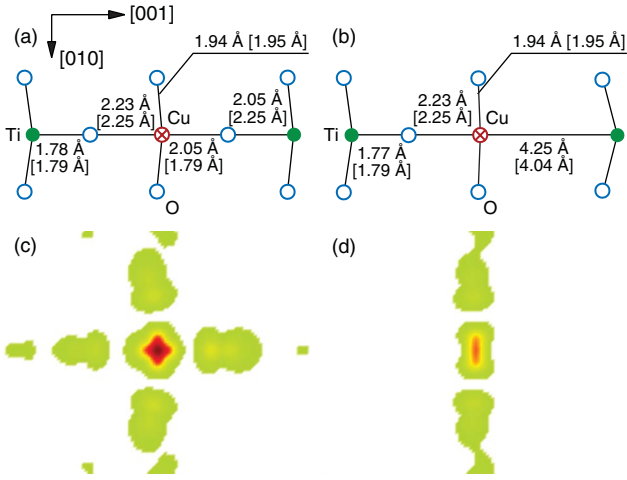


FIG. 2 (color). Isolated copper ion in charge state $q = -2$ (a),(b) and copper-oxygen vacancy complex of total charge state $q = 0$ (c),(d). (a),(c) Position of ions in the (100) plane containing the defect; numbers in square brackets report the equivalent distances in the defect-free crystal; (b),(d) spin-density patterns.

22.6% natural abundance bearing a nuclear spin of $I = \frac{1}{2}$. The values determined for $|a_{\text{iso}}| = \frac{|A_{\parallel}| + 2|A_{\perp}|}{3}$ and $|A'_{\parallel}| = \frac{|A_{\parallel}| - |A_{\perp}|}{3}$ for the “strong-coupling” quadrant and $|A'_{\parallel}| = \frac{4}{3}(2\nu_1\Delta\nu_s)^{(1/2)}$ for the “weak-coupling” quadrant based on the shift of the cross peaks by $\Delta\nu_s$ perpendicular to the $\nu_1 = -\nu_2$ antidiagonal [28] are listed in Table I for each set of correlations. The remaining features along the diagonal in the experimental HYSORE spectra are not due to weakly coupled nuclei with $\nu_{\alpha} \approx \nu_{\beta}$, but are rather a result of “combination peaks” or of incomplete inversion of the electron spin echo by the mixing π pulse. The HYSORE spectra exhibit features analogous to recently reported spectra for Cu^{2+} -modified PZT 54/46 compounds [14].

If one adopts the point-dipole approximation, the distances r between the Cu^{2+} ion and the ^{207}Pb nuclei can be determined using Eq. (2) in combination with the data for the dipolar ^{207}Pb hyperfine coupling also given in Table I. The measured hyperfine couplings and calculated distances for both strongly and weakly coupled lead nuclei

TABLE I. The ^{207}Pb -hyperfine couplings as obtained from the HYSORE spectra in Fig. 1(b) and distances between the copper functional center and neighboring lead nuclei obtained from the HYSORE measurements assuming a point-dipole approximation compared to distances obtained from the DFT calculations.

Coord. sphere	$ a_{\text{iso}}^{207\text{Pb}} $ (MHz)	$ A'_{\parallel} ^{207\text{Pb}} $ (MHz)	r_{HYSORE} (Å)	r_{DFT} (Å)
1	12.85 ± 0.05	1.90 ± 0.05	2.3 ± 1.0	3.15
2	2.95 ± 0.05	0.90 ± 0.05	2.9 ± 1.0	3.54
3	0.65 ± 0.05	0.15 ± 0.05	5.3 ± 1.0	[6.38; 6.89]

are summarized in Table I. On the basis of these distances, the couplings are assigned to ^{207}Pb nuclei in the first, second, and third coordination spheres. The measured ^{207}Pb -hyperfine parameters roughly correspond to data obtained from ^{207}Pb -ENDOR on Cu^{2+} impurity centers in a PbTiO_3 single crystal [29]. By taking the distance information into account, a structural arrangement of the Cu^{2+} functional center emerges, in which the Cu^{2+} ion relaxes back into the plane of equatorial oxygens, exactly probing the DFT-predicted quasicubic spin-density distribution. By comparing the experimentally determined distances with the distances from the DFT calculations, a systematic underestimation in the case of the experimental data should be taken into account [14]. This is due to the fact that the isotropic component of the ^{207}Pb -hyperfine interaction is much larger than the anisotropic one. This indicates that considerable spin density is transferred from the copper ion to the lead nuclei. As a result, anisotropic components due to local contributions of the $6p^1$ -type orbitals may occur. This effect will result in an overestimation of the dipolar hyperfine coupling and—depending on the sign of the hyperfine interaction—in an underestimation of the corresponding distances.

The charge and spin density obtained from the DFT calculations at farther ions—in particular at the nearest Pb^{2+} ions in the (110)-plane—have been analyzed. It is found that at these ions both the total charge density and the difference between the spin densities are nearly unaffected by the presence of the copper functional center and the resulting breaking of the translational symmetry.

Experimentally, the spin-density distribution at the lead nuclei can be mapped out by exploiting the orientation selective [30] ^{207}Pb -hyperfine interactions. As a function of orientation (not shown), no distinguishable difference could be observed, except a shift to higher frequencies with increasing field setting due to the dependence of the nuclear Zeeman interaction on the external field. Furthermore, the ^{207}Pb -hyperfine features and linewidths are identical for all observer field settings. In addition, for all three sets of correlation peaks, the isotropic part of the hyperfine splitting is considerably larger than the anisotropic part (see Table I). Hence, no orientation dependence with respect to the local coordinate system of the copper center is observed.

Extensive calculations on a variety of $(\text{Cu}_{\text{Ti}}-\text{V}_{\text{O}})$ defect associates show that there is a very strong chemical driving force for association of Cu impurities with oxygen vacancies. For the most stable configuration the binding energy ranges from 1.5 to 2.1 eV/defect pair depending on the Fermi energy [21]. As shown in Fig. 2(b), in this configuration the oxygen vacancy is located at the nearest O site along the [001] axis with respect to the Cu^{2+} ion. The most stable charge state is $(\text{Cu}_{\text{Ti}}''-\text{V}_{\text{O}}^{\bullet\bullet})^{\times}$. Compared to the isolated Cu impurity the displacement of the Cu^{2+} ion with respect to the nearest (001) plane of oxygen ions is further

diminished and amounts to merely 0.08 Å. The structural and electronic relaxation leads to the spin-density pattern shown in Fig. 2(d), which exhibits a pseudocubic symmetry. The DFT calculations hence provide evidence that a $(\text{Cu}_{\text{Ti}}''\text{-V}_{\text{O}}^{\bullet\bullet})^{\times}$ defect dipole is formed that is oriented along the crystallographic c axis. The orientation of the dipole is derived from both DFT results and the experimentally observed axially of the Cu^{2+} g matrix and $A^{63\text{Cu}}$ -hyperfine tensor. In case of an orientation of the dipole along the crystallographic a , b - axes, the site symmetry of the Cu^{2+} center would be lower than axial, in contradiction of the EPR results.

Combining all these results, a consistent picture of the prevailing defect structure for Cu^{2+} and Fe^{3+} functional centers in PbTiO_3 emerges, which provides support for the atomistic model suggested on the basis of macroscopic internal-field measurements for Ni^{2+} centers in BaTiO_3 [4,5]. Within this model, acceptor-type functional centers are assumed to form a defect dipole with a charge-compensating oxygen vacancy. Differences in the macroscopic piezoelectric properties of hard compounds doped with different acceptor ions may be explained on the basis of the corresponding electric dipole moment, considering the overall electric charge [neutral $(\text{Cu}_{\text{Ti}}''\text{-V}_{\text{O}}^{\bullet\bullet})^{\times}$ as compared to singly charged $(\text{Fe}_{\text{Ti}}'\text{-V}_{\text{O}}^{\bullet\bullet})^{\bullet}$ associates] or the corresponding “length” of the defect dipole.

In summary, the defect structure of the Cu^{2+} functional center in ferroelectric PbTiO_3 could be resolved by a combination of spectroscopic measurements with quantum mechanical calculations. The results show a strong chemical driving force for the formation of $(\text{Cu}_{\text{Ti}}''\text{-V}_{\text{O}}^{\bullet\bullet})^{\times}$ defect dipoles, in which the oxygen vacancy is located at the nearest O site along the tetragonal axis with respect to the copper functional center. The corresponding defect dipole is hence oriented in parallel with respect to the direction of spontaneous polarization. The present results contribute to a better understanding of defect association in ferroelectrics and the formation of defect dipoles, which pertain both to ferroelectric aging and electrical fatigue in piezoelectric materials.

This work has been supported by the DFG center of excellence No. 595 *Electric Fatigue in Functional Materials*. The authors are grateful to Professor Dr. David J. Keeble, for providing data from an ^{207}Pb -ENDOR study on the Cu^{2+} impurity center in a PbTiO_3 single crystal prior to publication. The use of a pulsed X-band spectrometer in the laboratory of Professor Dr. Klaus-Peter Dinse is acknowledged.

*eichel@chemie.tu-darmstadt.de

- [1] M.J. Hoffmann and H. Kungl, *Curr. Opin. Solid State Mater. Sci.* **8**, 51 (2004).
- [2] M. Dawber, K.M. Rabe, and J.F. Scott, *Rev. Mod. Phys.* **77**, 1083 (2005).
- [3] S. Pöykkö and D.J. Chadi, *Phys. Rev. Lett.* **83**, 1231 (1999).
- [4] H. Neumann and G. Arlt, *Ferroelectrics* **76**, 303 (1987).
- [5] G. Arlt and H. Neumann, *Ferroelectrics* **87**, 109 (1988).
- [6] W.L. Warren, D. Dimos, G.E. Pike, K. Vanheusden, and R. Ramesh, *Appl. Phys. Lett.* **67**, 1689 (1995).
- [7] W.L. Warren, G.E. Pike, K. Vanheusden, D. Dimos, B.A. Tuttle, and J. Robertson, *J. Appl. Phys.* **79**, 9250 (1996).
- [8] X. Ren, *Nat. Mater.* **3**, 91 (2004).
- [9] E. Siegel and K.A. Müller, *Phys. Rev. B* **19**, 109 (1979).
- [10] E. Siegel and K.A. Müller, *Phys. Rev. B* **20**, 3587 (1979).
- [11] H. Meštrić, R.-A. Eichel, T. Kloss, K.-P. Dinse, So. Laubach, St. Laubach, and P.C. Schmidt, *Phys. Rev. B* **71**, 134109 (2005).
- [12] H. Meštrić, R.-A. Eichel, K.-P. Dinse, A. Ozarowski, J. van Tol, L.C. Brunel, H. Kungl, M.J. Hoffmann, K.A. Schönau, M. Knapp, and H. Fuess, *Phys. Rev. B* **73**, 184105 (2006).
- [13] E. Erdem, R.-A. Eichel, H. Kungl, M.J. Hoffmann, A. Ozarowski, H. van Tol, and L.C. Brunel, *Phys. Scr.* **T129**, 12 (2007).
- [14] R.-A. Eichel, H. Kungl, and M.J. Hoffmann, *J. Appl. Phys.* **95**, 8092 (2004).
- [15] R.-A. Eichel, *J. Electroceram.* **19**, 9 (2007).
- [16] P. Höfer, A. Grupp, H. Nebenführ, and M. Mehring, *Chem. Phys. Lett.* **132**, 279 (1986).
- [17] C. Gemperle, G. Aebli, A. Schweiger, and R.R. Ernst, *J. Magn. Reson.* **88**, 241 (1990).
- [18] G. Kresse and J. Hafner, *Phys. Rev. B* **47**, 558 (1993); **49**, 14251 (1994); G. Kresse and J. Furthmüller, *ibid.* **54**, 11169 (1996); *Comput. Mater. Sci.* **6**, 15 (1996).
- [19] P.E. Blöchl, *Phys. Rev. B* **50**, 17953 (1994); G. Kresse and D. Joubert, *ibid.* **59**, 1758 (1999).
- [20] H.J. Monkhorst and J.D. Pack, *Phys. Rev. B* **13**, 5188 (1976).
- [21] P. Erhart, R.-A. Eichel, P. Träskelin, and K. Albe, *Phys. Rev. B* **76**, 174116 (2007).
- [22] R.-A. Eichel, H. Meštrić, K.-P. Dinse, A. Ozarowski, J. van Tol, L.C. Brunel, H. Kungl, and M.J. Hoffmann, *Magn. Reson. Chem.* **43**, S166 (2005).
- [23] D.J. Keeble, Z. Li, and M. Harmatz, *J. Phys. Chem. Solids* **57**, 1513 (1996).
- [24] W.L. Warren, B.A. Tuttle, F.C. Rong, G.J. Gerardi, and E.H. Poindexter, *J. Am. Ceram. Soc.* **80**, 680 (1997).
- [25] Z. Brykhar, I.P. Bykov, M.D. Glinchuk, V.V. Laguta, Y.L. Maximenko, Z. Potucek, L. Jastrabik, and H.J. Schulz, *Appl. Phys. A* **66**, 555 (1998).
- [26] H.T. Langhammer, T. Müller, R. Böttcher, and H.-P. Abicht, *Solid State Sci.* **5**, 965 (2003).
- [27] R.-A. Eichel, K.-P. Dinse, H. Kungl, M.J. Hoffmann, A. Ozarowski, J. van Tol, and L.C. Brunel, *Appl. Phys. A* **80**, 51 (2005).
- [28] A. Pöpll and L. Kevan, *J. Phys. Chem.* **100**, 3387 (1996).
- [29] D.J. Keeble (private communication).
- [30] G.H. Rist and J.S. Hyde, *J. Chem. Phys.* **52**, 4633 (1970).